

# Fast, higher-order direct/iterative hybrid solver for scattering by Inhomogeneous media – with application to high-frequency and discontinuous refractivity problems

Oscar P. Bruno\*      Ambuj Pandey\*

PRELIMINARY DRAFT

## Abstract

This paper presents a fast high-order method for the solution of two-dimensional problems of scattering by penetrable inhomogeneous media, with application to high-frequency configurations containing (possibly) discontinuous refractivities. The method relies on a combination of a differential volumetric formulation and a boundary integral formulation. Thus, in the proposed approach the entire computational domain is partitioned into large numbers of volumetric spectral approximation patches which are then grouped into patch subsets for local direct solution; the interactions with the exterior domain are handled by means of a boundary integral equation. The resulting algorithm can be quite effective: after a modestly-demanding precomputation stage (whose results for a given frequency can be repeatedly used for arbitrarily chosen incidence angles), the proposed algorithm can accurately evaluate scattering by configurations including large and complex objects and/or high refractivity contrasts, including possibly refractive-index discontinuities, in fast single-core runs.

## 1 Introduction

This paper considers the problem of evaluation of wave scattering by penetrable inhomogeneous media in the two dimensions. This is a problem of fundamental importance in a wide range of applications, including underwater acoustics [7] and biological and medical imaging [26] as well as seismology and geophysics [5, 32], among others. In all of these applications, it is highly desirable to utilize efficient and accurate numerical methods which can deal with arbitrary scattering geometries and (often discontinuous) refractive index distributions, even in the high-frequency regime. As is well known [20, 33, 34], this problem presents a number of challenges, as it requires use of large numbers of discretization points and, for iterative solvers, increasingly large numbers of iterations as the frequencies and/or refractive-index values increase. This paper proposes an algorithm which, relying on use of spectral approximation patches organized in a multilevel fashion and a boundary integral equation, together with, both, a multifrontal direct linear algebra solver [15] and the iterative solver GMRES, and leveraging a smoothing technique that yields second-order convergence even for discontinuous refractivities, can effectively solve challenging volumetric scattering problems in fast single-core runs.

---

\*Computing and Mathematical Sciences, Caltech, Pasadena, CA 91125, USA

Formally, the two dimensional forward scattering problem that we consider in this paper is described as follows: given an incident time-harmonic acoustic wave  $u^i$  satisfying free space Helmholtz equation

$$\Delta u^i(\mathbf{x}) + \kappa^2 u^i(\mathbf{x}) = 0, \quad \mathbf{x} \in \mathbb{R}^2 \quad (1)$$

and an open bounded inhomogeneities  $\mathcal{D} = \{\mathbf{x} : n(\mathbf{x}) \neq 1\} \subset \mathbb{R}^2$ , where  $\kappa$  is the wave number of the incoming wave  $u^i$  and  $n(\mathbf{x})$  is the index of refraction which assume value one in  $\mathbb{R}^2 \setminus \mathcal{D}$ , find the total acoustic field  $u$  that satisfies [14]

$$\Delta u(\mathbf{x}) + \kappa^2 n^2(\mathbf{x}) u(\mathbf{x}) = 0, \quad \mathbf{x} \in \mathbb{R}^2, \quad (2)$$

and the scattered field  $u^s := u - u^i$  satisfies Sommerfeld radiation condition

$$\lim_{r \rightarrow \infty} \sqrt{r} \left( \frac{\partial u^s}{\partial r} - i\kappa u^s \right) = 0, \quad (3)$$

uniformly in all directions, where  $r = (x_1^2 + x_2^2)^{1/2}$  and  $i = \sqrt{-1}$  is the imaginary unit. Throughout this paper it is assumed that  $n(\mathbf{x})$  in (2) is a positive piecewise continuous function throughout  $\mathbb{R}^2$ .

Broadly speaking, the numerical methods available for the solution of this problem fall into three different classes: (i) Differential equation based solvers; (ii) Integral equation based methods; and (iii) Solvers based on combination of differential and integral equation where integral evaluation required only on the boundary of computational domain.

Perhaps the simplest approach to solve the problem (2)-(3) is to replace the unbounded propagation domain by a bounded computational domain by introducing an artificial boundary containing the scatterer  $\mathcal{D}$  in its interior, and then solve the resulting problem by using finite element or finite difference methods. Unlike other methods, these approaches yield a sparse linear systems but in order to satisfy the radiation condition (3), they require use of absorbing boundary conditions of some sort. The classical absorbing-boundary techniques [9,17,21] generally require use of a relatively large computational domain for accuracy, and, thus, large number of unknowns and correspondingly large linear systems. More recent approaches [22], allow the use of absorbing boundaries that lie near the scattering boundaries domain at the expense of a degree of complexity in the algorithm. Additionally, finite-difference and finite-element method in case for equation (2) generally suffer from significant dispersion errors [6,8], and they lead to linear systems which require large numbers of iterations if treated by means of iterative linear algebra solvers [18,19].

Another widely used approach to obtain the numerical solution of (2)-(3) is to solve its equivalent *Lippmann-Schwinger* integral equation given by

$$u(\mathbf{x}) + \kappa^2 \int_{\mathcal{D}} G_{\kappa}(\mathbf{x} - \mathbf{y}) u(\mathbf{y}) m(\mathbf{y}) d\mathbf{y} = u^i(\mathbf{x}), \quad \mathbf{x} \in \mathbb{R}^2, \quad (4)$$

where  $G_{\kappa}(\mathbf{x}) = \frac{i}{4} H_0^1(\kappa|\mathbf{x}|)$ , is the radiating fundamental solution of Helmholtz equation in the free space and  $m(\mathbf{x}) = 1 - n^2(\mathbf{x})$  is the contrast function. This formulation offers several advantages; notably this approach only requires discretization of the scattering region  $\mathcal{D}$ ; and the solutions thus obtained automatically satisfy the Sommerfeld radiation condition (3). Additionally, equation (4) is a Fredholm equation of second kind, therefore, upon discretization, the condition number of the resulting linear system remains essentially constant as the discretization is refined. Unfortunately, however, volumetric scattering methods based on integral equation formulations give rise to certain difficulties, including

1. As in all integral solvers, a specialized quadrature rule must be used to integrate the integrand singularity accurately.
2. The resulting discrete linear systems are dense and non-Hermitian, and, thus, the solution of the resulting systems by means of direct linear-algebra techniques is impractical except for problems that are acoustically small.
3. A straightforward evaluation of the the action of the integral operator in (4) on the basis of an  $N$  point discretization, which could be used in conjunction with an iterative linear-algebra solver, requires a large computational cost, of order  $O(N^2)$  operations per iteration.
4. Equation (4) is known to require very large number of iterations for convergence whenever the frequency or the contrast function  $m(x)$  (or both) are large.

In recent years, a number of algorithms, including direct and iterative solvers, have been proposed for the solution of Lippmann-Schwinger equation, for instance, see [2, 4, 11, 12, 16, 27, 29, 30] and references therein. The simplest fast algorithms in this context, which relies on use of equidistant grids and FFTs, only provide first order convergence in presence of discontinuous index of refraction. For instance, the schemes introduced in [1, 16], provide fast high-order FFT-based methods for smooth refractivities, but they fail to produce high-order accuracy in presence of discontinuous refractive indices, and it requires large iteration numbers for high-frequencies and high refractivity contrast. The algorithm introduced in [11] exhibits second order convergence in the presence of discontinuous refractivity and has shown it’s applicability in dealing with some large frequency problems, but this approach does not address problem 4 above, and, once again, the algorithm requires large iteration numbers for large frequencies. The recent fast algorithms [3, 29] provide convergence-order higher than 2 via special treatment at discontinuity boundaries, but they also suffer from the problem described in point 4 above. Very recently preconditioning techniques with computational cost  $O(N^{3/2})$  were introduced in [28, 33, 34]. These preconditioners were shown to effectively reduce iteration numbers, even for high frequency problems. The performance of these methodologies is highly dependent on the smoothness of the refractive-index function. No reports have been provided in either theoretical, graphical or tabular form, on the numerical accuracy of the solutions provided by these methods. Additionally, reference [28, Sec. 2.5] indicates that “neither will the Nyström method be able to give an accurate discretization scheme nor can the sweeping factorization provide... an accurate approximating solution. Thus, for our preconditioner to work, we require certain smoothness from the velocity fields”.

Methods which, like the one proposed in this paper, are based on a combination of a volumetric differential formulation, as well as an integral equation formulation for the *physically exact* truncation of the computation domain, have also been proposed previously; see e.g. [24, 25] and references therein. A direct solver based on this general idea, with computational complexity of order  $O(N^{3/2})$ , was introduced in [20]. The method achieves its favorable operation count by decomposing the domain in a number of spectral square patches that are organized in a tree structure, with a subsequent aggregation process whereby, the Impedance-to-Impedance (ItI) maps of individual cells are recursively merged into ItI maps for larger and larger rectangular groups of cells. Ultimately, when the computational domain boundary is reached a boundary integral equation is used in conjunction with the Dirichlet-to-Neumann map (DtN) of the complete domain to enact the interactions between the bounded scatterer and the exterior domain. This algorithm can effectively treat high-frequency problems for which the refractivity is globally smooth—and, in particular,

smoothly reaches the vacuum refractive-index value 1 at the scatterer boundary. The method has not been applied to cases for which refractivity discontinuities exist, and it is expected that the first-order accuracy would ensue in such cases.

The approach proposed in this paper is a fast hybrid direct/iterative method which requires small numbers of iterations, which exhibits very low dispersion, and which, as discretizations are refined, converges with high-order accuracy for smooth refractivity, and with second-order accuracy (and low dispersion) in the discontinuous refractivity case. Our solver relies on a certain non-recursive multi-scale direct solution technique for the volumetric interior problem that, like the method [20], utilizes ItI maps between fine-scale spectral cells. But, unlike that contribution, the solution process in the present case is completed by (non-recursive) applications of ItI maps at three different levels, namely 1) Fine-scale cell groups; 2) Large-scale cell groups; and 3) Boundary cells. In the first two cases the necessary linear algebra solutions are obtained by means of the multifrontal solver [15]. The third step, which is tackled by means of the iterative linear-algebra solver GMRES, is enacted by incorporating a second-kind integral formulation in conjunction with an ItI map (instead of the possibly singular DtN used in [20]). In particular, the existence and uniqueness theory presented in the present paper, provides an affirmative answer to an open-question put forth in Section 6 of the latter contribution, concerning the existence of a second-kind formulation which involves only ItI maps, and not DtN maps.

As indicated in Section 3, the proposed hybrid direct/iterative strategy provides significant advantages over non-hybrid strategies where by either a fully iterative linear algebra solver is used, or a generic direct fast sparse solver such as [15] is utilized. Indeed, a fully iterative solver would necessarily require large numbers of iterations in order to account for the multiple scattering events that take place at boundaries of discontinuity of the refractive-index function  $n$ . But, as demonstrated in Section 4, the coupling to the boundary integral solver destroys the sparsity of the interior spectral solver, and thus renders a sparse solution strategy ineffective. The hybrid strategy achieves the dual goal of maintaining a low iteration count (since the boundary integral equation, which requires low iteration numbers, is only equation that is solved iteratively) while maintaining sparsity.

The overall proposed formulation can of course be used in conjunction with any adequate linear algebra solver for the volumetric portion of the algorithm, including the specialized Helmholtz direct linear-algebra solver proposed in [20]. The resulting approach would thus accomplish three goals which were left, in that reference, for future work, namely 1) Use of an exterior solver based on the ItI (instead of the Dirichlet-to-Neumann map); 2) Use of an overall formulation that is invertible for all frequencies; and 3) Utilization of a overall formulation based on an iterative strategy for the solution of the integral equation portion of the method. Alternatively, the present approach enables use of any efficient sparse linear algebra solver, and it additionally provides, for the first time, dispersionless higher-order convergence for discontinuous refractive index functions  $n$ .

To the best of our knowledge, this is the first solver which can provide fast and accurate solutions for high-frequency and/or high-contrast problems with discontinuous index of refraction while maintaining second order accuracy. We have organized this paper as follows: Section 2 contain some necessary preliminaries . Section 3 includes the detailed component of our algorithm. Further, to illustrate the performance of our algorithm numerical results are presented in section 4. Finally, a concluding remarks and a some possible directions for future research are discussed in section 5.

## 2 Uniquely-solvable, second-kind integro-differential hybrid formulation

As discussed in the previous section, the proposed numerical method is based on a reformulation of the problem (1)-(3) as a combination of a differential equation formulation in a volumetric region and a boundary integral equation formulation on the boundary of computational domain. To describe the method we consider an open bounded ‘‘computational’’ domain  $\Omega \subset \mathbb{R}^2$  (that may, in practice, be taken to equal a square or a rectangle) that contains the inhomogeneity:  $\overline{D} \subset \Omega$ . Then the complete problem (1)-(3) is reformulated in terms of two main elements: 1) A Helmholtz equation with variable coefficients in the volumetric region  $\Omega$  and; 2) A boundary integral equation on  $\partial\Omega$  which couples the solution within  $\Omega$  to the solution in the unbounded domain  $\mathbb{R}^2 \setminus \overline{\Omega}$ . In order to proceed with this plan the following section first discusses a certain impedance-to-impedance operators [20, 24, 25] associated with the Helmholtz problems inside and outside  $\Omega$ .

### 2.1 Interior and Exterior Impedance-to-Impedance operators

We define the interior and exterior impedance-to-impedance operators  $T_{\text{int}}$  and  $T_{\text{ext}}$ . In order to define the the operator  $T_{\text{int}} : H^{\frac{1}{2}}(\partial\Omega) \rightarrow H^{\frac{1}{2}}(\partial\Omega)$  we proceed as follows: given a function  $\phi \in H^{\frac{1}{2}}(\partial\Omega)$ ,  $T_{\text{int}}[\phi]$  is defined by

$$T_{\text{int}}[\phi](x) = \alpha u(\mathbf{x}) - i\kappa\beta \frac{\partial u}{\partial \boldsymbol{\nu}}(\mathbf{x}), \quad (5)$$

where  $u \in H^2(\Omega)$  is the solution of the problem

$$\Delta u(\mathbf{x}) + \kappa^2 n^2(\mathbf{x})u(\mathbf{x}) = 0, \quad \text{if } \mathbf{x} \in \Omega, \quad (6)$$

$$\alpha u(\mathbf{x}) + i\kappa\beta \frac{\partial u}{\partial \boldsymbol{\nu}}(\mathbf{x}) = \phi(\mathbf{x}), \quad \text{if } \mathbf{x} \in \partial\Omega, \quad (7)$$

where,  $\alpha, \beta \in \mathbb{R}$ . The definition of  $T_{\text{ext}} : H^{\frac{1}{2}}(\partial\Omega) \rightarrow H^{\frac{1}{2}}(\partial\Omega)$  is entirely analogous: for  $\phi \in H^{\frac{1}{2}}(\partial\Omega)$ ,  $T_{\text{ext}}[\phi]$  is defined by

$$T_{\text{ext}}[\phi](x) = \alpha u(\mathbf{x}) - i\kappa\beta \frac{\partial u}{\partial \boldsymbol{\nu}}(\mathbf{x}), \quad (8)$$

where  $u \in H_{\text{loc}}^2(\Omega)$  is a solution of the exterior problem

$$\Delta u(\mathbf{x}) + \kappa^2 n^2(\mathbf{x})u(\mathbf{x}) = 0, \quad \text{if } \mathbf{x} \in \mathbb{R} \setminus \Omega, \quad (9)$$

$$\alpha u(\mathbf{x}) + i\kappa\beta \frac{\partial u}{\partial \boldsymbol{\nu}}(\mathbf{x}) = \phi(\mathbf{x}), \quad \text{if } \mathbf{x} \in \partial\Omega. \quad (10)$$

### 2.2 Hybrid formulation

As is known [14, p. 70], the scattered field  $u^s$  over the exterior domain  $\mathbb{R}^2 \setminus \overline{\Omega}$  may be represented by means of the Green formula

$$u^s(\mathbf{x}) = \int_{\partial\Omega} \left( \frac{\partial G_\kappa(\mathbf{x} - \mathbf{y})}{\partial \boldsymbol{\nu}(\mathbf{y})} u(\mathbf{y}) - G_\kappa(\mathbf{x} - \mathbf{y}) \frac{\partial u}{\partial \boldsymbol{\nu}}(\mathbf{y}) \right) ds(\mathbf{y}), \quad \mathbf{x} \in \mathbb{R}^2 \setminus \overline{\Omega}. \quad (11)$$

Further, utilizing the jump relations of the single- and double-layer potentials on  $\partial\Omega$  we obtain

$$u^s(\mathbf{x}) = \frac{u(\mathbf{x})}{2} + \int_{\partial\Omega} \left( \frac{\partial G_\kappa(\mathbf{x} - \mathbf{y})}{\partial \boldsymbol{\nu}(\mathbf{y})} u(\mathbf{y}) - G_\kappa(\mathbf{x} - \mathbf{y}) \frac{\partial u}{\partial \boldsymbol{\nu}}(\mathbf{y}) \right) ds(\mathbf{y}), \quad \mathbf{x} \in \partial\Omega. \quad (12)$$

In view of the continuity of  $u$  and  $\frac{\partial u}{\partial \boldsymbol{\nu}}$  across  $\partial\Omega$  we see that the total field  $u$  satisfies the following hybrid problem on  $\overline{\Omega}$ :

$$\Delta u(\mathbf{x}) + \kappa^2 n^2(\mathbf{x}) u(\mathbf{x}) = 0, \quad \text{if } \mathbf{x} \in \Omega, \quad (13)$$

$$\phi - \left( \alpha u(\mathbf{x}) + i\kappa\beta \frac{\partial u}{\partial \boldsymbol{\nu}}(\mathbf{x}) \right) = 0, \quad \text{if } \mathbf{x} \in \partial\Omega, \quad (14)$$

$$\frac{1}{4\alpha} (I + T_{\text{int}}) [\phi](\mathbf{x}) - \mathcal{A}_{\text{ext}}^{\text{int}}[\phi](\mathbf{x}) = u^i(\mathbf{x}) \quad \text{for } \mathbf{x} \in \partial\Omega, \quad (15)$$

where

$$\mathcal{A}_{\text{ext}}^{\text{int}}[\phi](\mathbf{x}) = \int_{\partial\Omega} \left( \frac{1}{2\alpha} \frac{\partial G_\kappa(\mathbf{x} - \mathbf{y})}{\partial \boldsymbol{\nu}(\mathbf{y})} (I + T_{\text{int}}) [\phi](\mathbf{y}) - \frac{1}{2i\kappa\beta} G_\kappa(\mathbf{x} - \mathbf{y}) (I - T_{\text{int}}) [\phi](\mathbf{y}) \right) ds(\mathbf{y}). \quad (16)$$

is the Green formula in the *exterior* of  $\Omega$  (that is, for  $\mathbf{x} \in \mathbb{R}^2 \setminus \overline{\Omega}$ ) on the basis of the *interior* ItI map  $T_{\text{int}}$ .

It is easy to check that, given a solution of (2)-(3) and defining  $\phi = \alpha u + i\kappa\beta \frac{\partial u}{\partial \boldsymbol{\nu}}$ , the pair of functions  $(u, \phi)$  is a solution of the problem (13)–(15). As shown in the following section, further, the problem (13)–(15) is uniquely solvable—and its solution must therefore coincide with the restriction to  $\Omega$  of the solution of the original inhomogeneous scattering problem 1–3. Once the solution of (13)–(15) is obtained for  $\mathbf{x} \in \Omega$ , the scattered field  $u^s$  (and hence the total field  $u = u^i + u^s$ ) at any point  $\mathbf{x} \in \mathbb{R}^2 \setminus \overline{\Omega}$  can be easily obtained by utilizing the representation formula (11). In other words, the hybrid integro-differential problem (13)–(15) is equivalent to the original inhomogeneous scattering problem (2)-(3), as claimed.

## 2.3 Uniqueness

**Theorem 1** (Uniqueness of solution for the second-kind hybrid volume-boundary formulation). *Let  $(u, \phi) \in H^2(\Omega) \times H^{\frac{1}{2}}(\partial\Omega)$  denote a solution of (13)–(15) with  $u^i = 0$  on  $\partial\Omega$ . Then  $(u, \phi) = (0, 0)$ .*

*Proof.* Let  $(u, \phi)$  denote a solution of (13)–(15) with  $u^i = 0$ . Using the given function  $\phi \in H^{\frac{1}{2}}(\partial\Omega)$ , let  $u_{\text{ext}} \in H_{\text{loc}}^2(\mathbb{R}^2 \setminus \Omega)$  denote the radiating solution of the uniquely solvable problem

$$\Delta u_{\text{ext}}(\mathbf{x}) + \kappa^2 u_{\text{ext}}(\mathbf{x}) = 0, \quad \text{if } \mathbf{x} \in \mathbb{R}^2 \setminus \overline{\Omega}, \quad (17)$$

$$\alpha u_{\text{ext}}(\mathbf{x}) + i\kappa\beta \frac{\partial u_{\text{ext}}}{\partial \boldsymbol{\nu}}(\mathbf{x}) = \phi, \quad \text{if } \mathbf{x} \in \partial\Omega. \quad (18)$$

Using the exterior ItI operator  $T_{\text{ext}}$  defined in (8) together with the Green representation formula (11) for  $u_{\text{ext}}$  we obtain

$$\frac{1}{4\alpha} (I + T_{\text{ext}}) [\phi](\mathbf{x}) - \mathcal{A}_{\text{ext}}^{\text{ext}}[\phi](\mathbf{x}) = 0 \quad \text{for } \mathbf{x} \in \partial\Omega, \quad (19)$$

where

$$\mathcal{A}_{\text{ext}}^{\text{ext}}[\phi](\mathbf{x}) = \int_{\partial\Omega} \left( \frac{1}{2\alpha} \frac{\partial G_{\kappa}(\mathbf{x} - \mathbf{y})}{\partial \boldsymbol{\nu}(\mathbf{y})} (I + T_{\text{ext}})[\phi](\mathbf{y}) - \frac{1}{2i\kappa\beta} G_{\kappa}(\mathbf{x} - \mathbf{y}) (I - T_{\text{ext}})[\phi](\mathbf{y}) \right) ds(\mathbf{y}). \quad (20)$$

is the Green formula in the *exterior* of  $\Omega$  on the basis of the *exterior* ItI map  $T_{\text{ext}}$ .

Equation (15) and (19) can be recast in the forms

$$\frac{T_{\text{int}}[\phi](\mathbf{x})}{2} - \int_{\partial\Omega} \left( \frac{\partial G_{\kappa}(\mathbf{x} - \mathbf{y})}{\partial \boldsymbol{\nu}(\mathbf{y})} - i\eta G_{\kappa}(\mathbf{x} - \mathbf{y}) \right) T_{\text{int}}[\phi](\mathbf{y}) ds(\mathbf{y}) = f_{\phi}(\mathbf{x}), \quad \mathbf{x} \in \partial\Omega, \quad (21)$$

$$\frac{T_{\text{ext}}[\phi](\mathbf{x})}{2} - \int_{\partial\Omega} \left( \frac{\partial G_{\kappa}(\mathbf{x} - \mathbf{y})}{\partial \boldsymbol{\nu}(\mathbf{y})} - i\eta G_{\kappa}(\mathbf{x} - \mathbf{y}) \right) T_{\text{ext}}[\phi](\mathbf{y}) ds(\mathbf{y}) = f_{\phi}(\mathbf{x}), \quad \mathbf{x} \in \partial\Omega, \quad (22)$$

where

$$f_{\phi}(\mathbf{x}) = -\frac{\phi}{2} + \int_{\partial\Omega} \left( \frac{\partial G_{\kappa}(\mathbf{x} - \mathbf{y})}{\partial \boldsymbol{\nu}(\mathbf{y})} + i\eta G_{\kappa}(\mathbf{x} - \mathbf{y}) \right) \phi(\mathbf{y}) ds(\mathbf{y}) \quad (23)$$

and  $\eta = \alpha/\kappa\beta$ . Clearly, Equations (21) and (22) are combined field integral equation of second kind for the unknowns  $T_{\text{ext}}[\phi]$  and  $T_{\text{int}}[\phi]$  with same right hand side. Since, as is well known [14, p. 51], these combined field integral equation admit unique solutions. Thus

$$T_{\text{int}}[\phi] = T_{\text{ext}}[\phi] \quad \text{or, equivalently} \quad \alpha u(\mathbf{x}) - i\kappa\beta \frac{\partial u}{\partial \boldsymbol{\nu}}(\mathbf{x}) = \alpha u_{\text{ext}}(\mathbf{x}) - i\kappa\beta \frac{\partial u_{\text{ext}}}{\partial \boldsymbol{\nu}}(\mathbf{x}) \quad \text{on } \partial\Omega. \quad (24)$$

But, from (14) and (18) we see that

$$\alpha u(\mathbf{x}) + i\kappa\beta \frac{\partial u}{\partial \boldsymbol{\nu}}(\mathbf{x}) = \phi = \alpha u_{\text{ext}}(\mathbf{x}) + i\kappa\beta \frac{\partial u_{\text{ext}}}{\partial \boldsymbol{\nu}}(\mathbf{x}),$$

and, therefore, using (24) it follows that

$$u = u_{\text{ext}} \quad \text{and} \quad \frac{\partial u}{\partial \boldsymbol{\nu}} = \frac{\partial u_{\text{ext}}}{\partial \boldsymbol{\nu}} \quad \text{on } \partial\Omega. \quad (25)$$

Let us now define

$$U_{\phi}(\mathbf{x}) = \begin{cases} u(\mathbf{x}) & \text{if } \mathbf{x} \in \bar{\Omega} \\ u_{\text{ext}}(\mathbf{x}) & \text{otherwise.} \end{cases} \quad (26)$$

In view (13), (17), and (25), and since  $u_{\text{ext}}$  is a radiating solution at infinity, it follows that  $U_{\phi}$  is radiating solution of the inhomogeneous Helmholtz problem (1)-(3) with throughout  $\mathbb{R}^2$  with  $u^i = 0$ , and hence,  $U_{\phi}$  must vanish identically—in view of the uniqueness [14] of  $H_{\text{loc}}^2$  solution of the inhomogeneous problem (1)-(3). In particular, it follows that  $u = 0$  in  $\Omega$  and, thus,  $\phi = 0$  on  $\partial\Omega$ , and the proof follows.  $\square$

Having established the well posedness of the second-kind hybrid formulation (13)-(15), the next section presents the proposed numerical algorithm for the solution of the hybrid volumetric integro-differential formulation (13)–(15).

### 3 Numerical algorithm

Following the algorithm outline presented in Section 2, let  $\Omega = (-a, a)^2$  denote a square computational domain such that  $\overline{\mathcal{D}} \subset \Omega$ . As indicated in Sections 1 and 2, the proposed algorithm consists of two main components, namely 1) A spectral volumetric solver for the Boundary Value Problem (BVP) (13)–(14) in the domain  $\Omega$  with given impedance data  $\phi \in H^{1/2}(\partial\Omega)$ ; and 2) A solver for the boundary integral equation (15) on  $\partial\Omega$ , which couples the solution within  $\Omega$  to the solution in the exterior of that domain. (In order to achieve second-order convergence for discontinuous scatterers the algorithm utilizes a Fourier-smoothing technique outlined in Section 3.1.1) The overall hybrid approach is completed via an application of the iterative solver GMRES, as detailed in Section 3.3. As mentioned in Section 1 the overall hybrid method meets the dual goals of achieving low iteration numbers while maintaining the sparsity of the spectral matrix.

#### 3.1 Volumetric boundary-value solver

In this section we describe our discretization and direct solution strategy for the BVP (13)–(14) for given values of the impedance  $\phi$  on  $\partial\Omega$ . The presentation includes five subsections, covering Fourier smoothing to enable second-order convergence even for discontinuous scatterers (Section 3.1.1); Large-scale partitioning strategy into rectangular subdomains (Section 3.1.2); Fine-scale partitioning and Chebyshev discretization of rectangular subdomains (Section 3.1.3); Mapping of overall impedance data into impedance data over the rectangular subdomain boundaries (Section 3.1.4), and, finally, algorithmic description that orchestrates the aforementioned components into an accurate and effective boundary value solver.

##### 3.1.1 Fourier smoothing of discontinuous refractivity

First we point out that, by our uniqueness proof of the formulation (13)–(15), Lippmann-Schwinger integral equation (4) is also equivalent to the problem (13)–(15). Algorithm presented in [23], achieved second order convergence for the solution of the problem (2)–(3) by solving its equivalent integral equation formulation 4. The key idea behind quadratic convergence rate was the replacement of discontinuous contrast function  $m(\mathbf{x}) = 1 - n^2(\mathbf{x})$  by its truncated Fourier series with the assumption that corresponding Fourier coefficients are either known analytically or can be computed very accurately. As the problem (13)–(15) is equivalent to (4), and therefore, same behavior is expected when similar treatment will be incorporated for the solution of the problem (13)–(15). And, indeed, we will show in the numerical results, after incorporating this idea we are getting second order convergence.

To apply this idea, we rewrite the equation (13) as

$$\Delta u(\mathbf{x}) + \kappa^2(1 - m(\mathbf{x}))u(\mathbf{x}) = 0. \quad (27)$$

While the contrast function  $m(\mathbf{x})$  is discontinuous in the computational domain  $\Omega$  but it is also compactly supported and piece-wise smooth in  $\Omega$ . Therefore, Fourier series of  $m(\mathbf{x})$  will uniformly converges to  $m(\mathbf{x})$  except at the region of discontinuity where it has sharp oscillations due to Gibbs artifact. By  $m^F(\mathbf{x})$ , we denote the truncated Fourier series of  $m$  in  $\Omega$  of period  $2a$  in each dimension and that can be read as

$$m^F(\mathbf{x}) = \sum_{\ell_1=-F}^F \sum_{\ell_2=-F}^F c_{\ell_1, \ell_2} e^{\frac{\pi i}{a}(\ell_1 x_1 + \ell_2 x_2)}, \quad (28)$$

where  $\mathbf{x} = (x_1, x_2)$  and the Fourier coefficient  $c_{\ell_1, \ell_2}$  is given by

$$c_{\ell_1, \ell_2} = \frac{1}{4a^2} \int_{-a}^a \int_{-a}^a m(x_1, x_2) e^{-\frac{\pi i}{a}(\ell_1 x_1 + \ell_2 x_2)} dx_1 dx_2. \quad (29)$$

We assume that, coefficients  $c_{\ell_1, \ell_2}$  is known with high accuracy. Direct use of FFT for its computation is not recommended as it will give poor approximation owing to discontinuity  $m(\mathbf{x})$  in the integration region  $[-a, a]^2$ . A fast and accurate algorithm for evaluation of these Fourier coefficients will be included in the final arXiv and archival versions of this manuscript. Now in equation (27), we replace the function  $m(\mathbf{x})$  by its truncated Fourier series  $m^F(\mathbf{x})$  in  $\Omega$  (with highly accurate Fourier coefficients!) to obtain

$$\Delta u(\mathbf{x}) + \kappa^2(1 - m^F(\mathbf{x}))u(\mathbf{x}) = 0. \quad (30)$$

Now, in the scattering formulation (13)–(15), we replace equation (13) by (30) and the numerical solution of newly introduced formulation yield second order convergent solution to the original problem (13)–(15), in spite of the low order approximation of  $m(\mathbf{x})$  by  $m^F(\mathbf{x})$  and associated Gibbs errors. Unlike the algorithm in [23], our gridding strategy is not equidistant, therefore, a straight forward evaluation of  $m^F(\mathbf{x})$  at  $N$  points results in an order  $O(NF^2)$  computational cost. One can easily expedite this computation by using FFT-refined trigonometric polynomial interpolation introduced in [13] which is known to be high-order accurate while maintaining computational efficiency and that we summarize as the following three step procedure:

1. Obtain the Fourier coefficients  $c_{\ell_1, \ell_2}$  accurately.
2. Evaluate the Fourier series  $m^F(\mathbf{x})$  on much finer equidistant Cartesian grids. This step can be easily performed using FFT by zero padding in the summation (28).
3. Construct local interpolating polynomials of a fixed degree using values  $m^F(\mathbf{x})$  at finer grids obtained in Step 2.

This procedure yield accurate interpolating polynomial that require negligible cost in contrast to the total computational cost of the algorithm.

### 3.1.2 Volumetric discretization

This section presents the proposed direct solution strategy for the numerical solution of boundary value problem (BVP) (13)–(14). As mentioned in the previous subsection, to deal with possible discontinuities in the refractivity  $n(\mathbf{x})$ , instead of BVP (13)–(14), the following modified BVP

$$\Delta u(\mathbf{x}) + \kappa^2 (1 - m^F(\mathbf{x})) u(\mathbf{x}) = 0, \quad \text{if } \mathbf{x} \in \Omega, \quad (31)$$

$$\alpha u(\mathbf{x}) + i\kappa\beta \frac{\partial u}{\partial \boldsymbol{\nu}}(\mathbf{x}) = \phi \quad \text{if } \mathbf{x} \in \partial\Omega \quad (32)$$

is solved—which leads to second-order accurate approximations to the actual solutions of the original problem (13)–(14). For the discussion in the present section we assume that the impedance data  $\phi$  in equation (32) is known on  $\partial\Omega$ .

We wish to utilize a general purpose fast sparse direct solver, such as, e.g., the multifrontal algorithm [15], for the solution of linear system arising as a result of discretization of BVP (31)-(32).

The performance of these solvers is highly dependent on the sparsity pattern of the coefficient matrix of the linear system. In view of this, we seek to approximate all necessary differential operators in such a way that the resulting linear system is sparse. To obtain accurate solutions even for large scale problems while maintaining sparsity we approximate the unknown functions  $u$  and its needed derivatives by using local Chebyshev representations. The desired local approximations and sparsity are achieved by breaking the problem (31)-(32) into a multiple boundary value problems in the smaller subdomains contained in the overall computational domain  $\Omega$ . The proposed algorithm for the BVP solution is described in the rest of this section.

The proposed BVP solver proceeds by first splitting the complete computational domain  $\Omega$  into  $K^2$  square subdomains  $\Omega^{p,q}$ ,  $p, q = 1, \dots, K$  such that  $\Omega^{p,q} \subset \Omega$ , so that

$$\Omega = \bigcup_{p=1}^K \bigcup_{q=1}^K \Omega^{p,q}.$$

Let  $u^{p,q} = u|_{\Omega^{p,q}}$ ,  $\frac{\partial u^{p,q}}{\partial \boldsymbol{\nu}} = \frac{\partial u}{\partial \boldsymbol{\nu}}|_{\partial\Omega^{p,q}}$ . Now, we recast the problem (31)-(32) on each of the subdomains  $\Omega^{p,q} \subset \Omega$  as

$$\Delta u^{p,q}(\mathbf{x}) + \kappa^2(1 - m^F(\mathbf{x}))u^{p,q}(\mathbf{x}) = 0, \quad \text{if } \mathbf{x} \in \Omega^{p,q}, \quad (33)$$

$$\alpha u^{p,q}(\mathbf{x}) + i\kappa\beta \frac{\partial u^{p,q}}{\partial \boldsymbol{\nu}}(\mathbf{x}) = \phi^{p,q}(\mathbf{x}) \quad \text{if } \mathbf{x} \in \partial\Omega^{p,q}, \quad (34)$$

where the function  $\phi^{p,q}$  on  $\partial\Omega_{p,q}$  is the unknown which we wish to determine. At the common boundary of each sub-domain the solution satisfies the transmission boundary conditions: the solution and its normal derivative is continuous across the common boundary. Boundary impedance data  $\phi^{p,q}$  for each subdomain will be obtained from the global impedance data  $\phi$  on  $\partial\Omega$  and transmission conditions along the common boundaries, as discussed below. To obtain, fast, accurate and dispersionless approximation of the BVP (33)-(34), we utilize local approximations of  $u$  by Chebyshev polynomials—as described in what follows.

### 3.1.3 Chebyshev patching, discretization and local approximations

For each  $p, q$  the subdomain  $\Omega^{p,q}$  is decomposed into a number of mutually disjoint square patches  $\Omega_{i,j}^{p,q}$ ,  $1 \leq i, j \leq L$  such that  $\Omega_{i,j}^{p,q} \subset \Omega_{p,q}$  and

$$\Omega^{p,q} = \bigcup_{i=1}^L \bigcup_{j=1}^L \Omega_{i,j}^{p,q}.$$

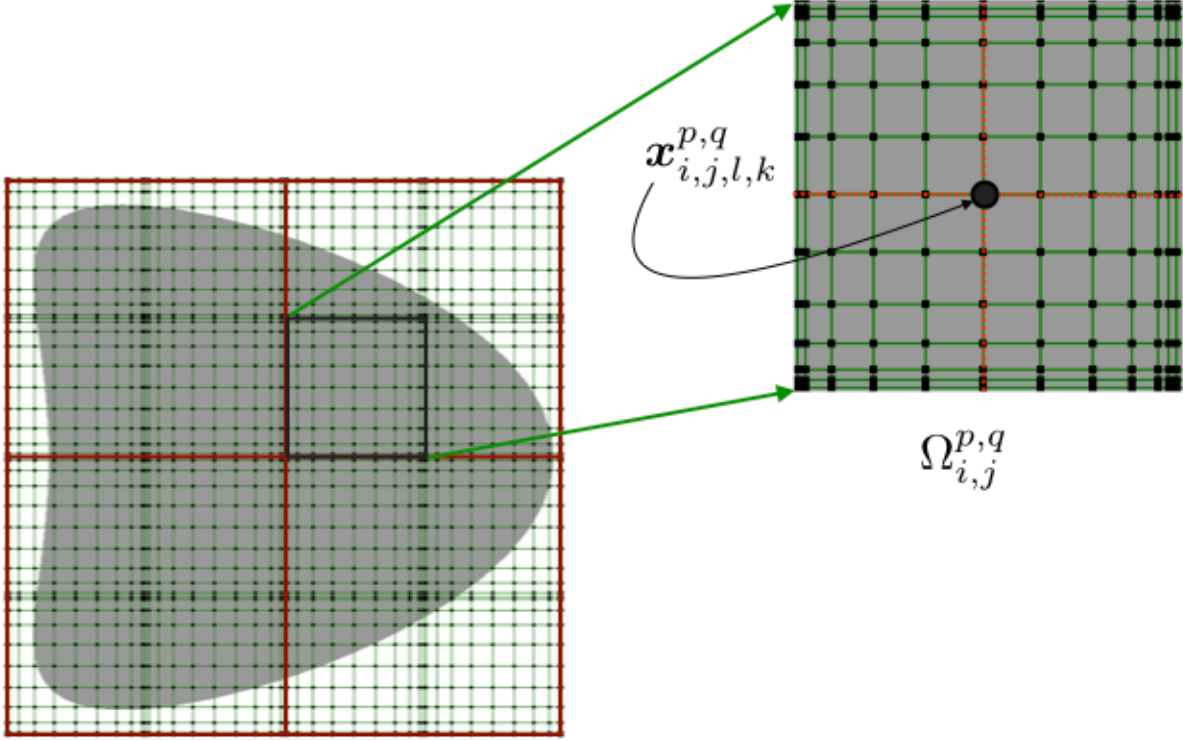


Figure 1: Computational domain  $\Omega$  containing the inhomogeneity  $\mathcal{D}$  and divided into four subdomains. In this example, each subdomain is further subdivided into four Chebyshev patches. In each patch, derivatives at a given point are approximated on the basis of function values along the line passing through that point.

Now, for each  $p, q$ , we re-formulate the boundary value problem (33)-(34) as

$$\Delta u_{i,j}^{p,q}(\mathbf{x}) + \kappa^2(1 - m^F(\mathbf{x}))u_{i,j}^{p,q}(\mathbf{x}) = 0, \quad \text{if } \mathbf{x} \in \Omega_{i,j}^{p,q}, \quad (35)$$

$$\alpha u_{i,j}^{p,q}(\mathbf{x}) + i\kappa\beta \frac{\partial u_{i,j}^{p,q}}{\partial \boldsymbol{\nu}}(\mathbf{x}) = \begin{cases} \alpha u_{i-1,j}^{p,q}(\mathbf{x}) + i\kappa\beta \frac{\partial u_{i-1,j}^{p,q}}{\partial \boldsymbol{\nu}}(\mathbf{x}) & \text{if } \mathbf{x} \in \partial\Omega_{i,j}^{p,q} \cap \partial\Omega_{i-1,j}^{p,q}, \\ \alpha u_{i+1,j}^{p,q}(\mathbf{x}) + i\kappa\beta \frac{\partial u_{i+1,j}^{p,q}}{\partial \boldsymbol{\nu}}(\mathbf{x}) & \text{if } \mathbf{x} \in \partial\Omega_{i,j}^{p,q} \cap \partial\Omega_{i+1,j}^{p,q}, \\ \alpha u_{i,j-1}^{p,q}(\mathbf{x}) + i\kappa\beta \frac{\partial u_{i,j-1}^{p,q}}{\partial \boldsymbol{\nu}}(\mathbf{x}) & \text{if } \mathbf{x} \in \partial\Omega_{i,j}^{p,q} \cap \partial\Omega_{i,j-1}^{p,q}, \\ \alpha u_{i,j+1}^{p,q}(\mathbf{x}) + i\kappa\beta \frac{\partial u_{i,j+1}^{p,q}}{\partial \boldsymbol{\nu}}(\mathbf{x}) & \text{if } \mathbf{x} \in \partial\Omega_{i,j}^{p,q} \cap \partial\Omega_{i,j+1}^{p,q}, \\ \phi^{p,q}(\mathbf{x}), & \text{if } \mathbf{x} \in \partial\Omega_{i,j}^{p,q} \cap \partial\Omega^{p,q}. \end{cases} \quad (36)$$

where  $u_{i,j}^{p,q} = u^{p,q}|_{\Omega_{i,j}^{p,q}} = u|_{\Omega_{i,j}^{p,q}}$ ,  $\frac{\partial u_{i,j}^{p,q}}{\partial \boldsymbol{\nu}} = \frac{\partial u^{p,q}}{\partial \boldsymbol{\nu}}|_{\partial\Omega_{i,j}^{p,q}} = \frac{\partial u}{\partial \boldsymbol{\nu}}|_{\partial\Omega_{i,j}^{p,q}}$  and where  $\boldsymbol{\nu}$  denotes the outward unit normal vector.

We discretize the square patch  $\Omega_{i,j}^{p,q} = [a_{i,j}^{p,q}, b_{i,j}^{p,q}]^2 \subset \Omega$  by a tensor product

$$\mathcal{N}_{i,j}^{p,q} = \{ \mathbf{x}_{i,j,\ell,k}^{p,q} | 0 \leq \ell \leq n_1, 0 \leq k \leq n_2 \},$$

of one dimensional Chebyshev meshes, where

$$\mathbf{x}_{i,j,\ell,k}^{p,q} = \left( \frac{a_{i,j}^{p,q} + b_{i,j}^{p,q}}{2} + \frac{b_{i,j}^{p,q} - a_{i,j}^{p,q}}{2} \cos\left(\frac{\pi\ell}{n_1}\right), \frac{a_{i,j}^{p,q} + b_{i,j}^{p,q}}{2} + \frac{b_{i,j}^{p,q} - a_{i,j}^{p,q}}{2} \cos\left(\frac{\pi k}{n_2}\right) \right).$$

Thus, the computational grid in the subdomain  $\Omega^{p,q}$  is given by

$$\mathcal{N}^{p,q} = \bigcup_{i=0}^L \bigcup_{j=0}^L \mathcal{N}_{i,j}^{p,q}$$

and the overall grid points in the computational domain  $\Omega$  is obtained as

$$\mathcal{N} = \bigcup_{p=0}^K \bigcup_{q=0}^K \mathcal{N}^{p,q}.$$

We denote the cardinality of the set  $\mathcal{N}_{i,j}^{p,q}, \mathcal{N}^{p,q}, \mathcal{N}$  by  $N_{i,j}^{p,q}, N^{p,q}, N$  respectively. At each grid point  $\mathbf{x}_{i,j,\ell,k}^{p,q}$ , we approximate the differential operators  $\partial/\partial x$ ,  $\partial/\partial y$  and  $\Delta$  by spectral differentiation matrices local to the patch  $\Omega_{i,j}^{p,q}$ . Note that, in this approximation the only non-zero entries are those which lie on the line passing through the point  $\mathbf{x}_{i,j,\ell,k}^{p,q}$ . A pictorial illustration of this presented in Figure 1. These approximations of derivatives by Chebyshev polynomial not only provide accurate approximations even for large wavenumbers, but also, when used for discretization of (35)-(36), give rise to sparse linear systems—suitable for treatment by sparse linear solvers such as the multifrontal-based direct solver [15].

### 3.1.4 Approximation of impedance data on the subdomain boundaries

In each subdomain  $\Omega^{p,q}$ , BVP (35)–(36) can be solved by means of the method described in the previous subsection provided the impedance data  $\phi^{p,q}(x)$  is known on the boundary  $\partial\Omega^{p,q}$ . In this section, we describe our algorithm for the computation of  $\phi^{p,q}$  on  $\partial\Omega^{p,q}$ .

Let  $\mathcal{N}_c$  denote the set of all grid points over all of the subdomain boundaries  $\partial\Omega^{p,q}$ , that is,

$$\mathcal{N}_c = \mathcal{N} \cap \Gamma \quad \text{where} \quad \Gamma = \bigcup_{p=0}^F \bigcup_{q=0}^F \partial\Omega^{p,q}. \quad (37)$$

We denote the cardinality of  $\mathcal{N}, \mathcal{N}_c$  by  $N$  and  $N_c$  respectively. Let  $\mathbf{g}$  denote a vector whose entries are the unknown impedance values  $\phi^{p,q}(\mathbf{x})$  over all points in the discretization  $\mathcal{N}_c$ .

We obtain the unknown vector  $\mathbf{g}$  on  $\Gamma$  by solving the linear system

$$\mathbf{A}\mathbf{g} = \mathbf{b}, \quad (38)$$

where  $\mathbf{A}$  is an  $N_c \times N_c$  square matrix and  $\mathbf{b}$  is  $N_c \times 1$  vector whose equal zero, except for those which correspond to the grid points lying on  $\partial\Omega$ . Our methodology yields a sparse matrix  $\mathbf{A}$ , and therefore, equation (38) can be solved by means of a sparse linear algebra solver. Since the proposed approach requires solutions of the system (38) for multiple right-hand sides, our algorithm computes the LU factorization of this matrix once and stores it for repeated use.

The construction of the matrix  $\mathbf{A}$  is straightforward, but this step is the most expensive part of the proposed method. To obtain the  $j^{\text{th}}$  column  $\mathbf{A}_j$  of the matrix  $\mathbf{A}$  we utilize impedance data  $\phi$  given by canonical basis vector  $\mathbf{e}_j$  of length  $N_c \times 1$  whose  $j^{\text{th}}$  all of whose entries vanish except of the  $j$ -th one which is equal to one, and we solve the BVP (33)-(34) in each subdomain. We note that, as the impedance data  $\mathbf{e}_j$  vanishes at the boundary of most subdomains, an actual solution procedure needs only be performed in subdomains which contain a non-zero vector on the right-hand side. Once we obtain the solution in the interior and boundary of subdomain we can easily compute the Neumann data and hence impedance data on the interface  $\partial\Omega^{p,q}$ . We connect the solution of all

subdomain by imposing continuity of impedance data on the interface of each pair of neighboring subdomains. Then we construct the column vector  $\mathbf{A}_j$  of  $\mathbf{A}$  as follows: those entries of  $\mathbf{A}_j$  which correspond to the unknown on  $\partial\Omega$  coincide with those in  $\mathbf{e}_j$ , and the remaining ones are equal to the difference of impedance data on  $\partial\Omega^{p,q}$  coming from neighboring subdomains. We repeat this process for each  $j = 1, \dots, N_c$  and thus obtain the full matrix  $\mathbf{A}$ .

### 3.1.5 Volumetric solver: algorithm

The main components of the proposed solver algorithm can be summarized as follows.

1. For each  $p, q = 1, \dots, K$ , construct a matrix  $\mathbf{A}_{p,q}$  using the algorithm described in Section 3.1.3.
2. Corresponding to each discretization point  $\mathbf{x}_j \in \Gamma$ , take a canonical vector  $\mathbf{e}_j$  of size  $N_c \times 1$  such that the  $j^{\text{th}}$  entry equals one and the rest equal zero. Then, by using the vector  $\mathbf{e}_j$  as impedance data on  $\Gamma$ , extract the impedance data on  $\partial\Omega_{p,q}$ , which will be denoted by  $\boldsymbol{\psi}_{p,q}$ .
3. If  $\boldsymbol{\psi}_{p,q}$  is not a zero vector then compute the solution of the linear system

$$\mathbf{A}_{p,q} \mathbf{U}_{p,q} = \mathbf{b}_{p,q},$$

where  $\mathbf{b}_{p,q} = (\boldsymbol{\psi}_{p,q}, \mathbf{0})$ . Perform this step for each  $p, q = 1, \dots, K$ .

4. Impose the continuity of the impedance data across the common boundaries of each pair of neighboring subdomains  $\Omega_{p,q}$  and save the resulting vector as a  $j^{\text{th}}$  column vector, say  $\mathbf{A}_j$  of matrix  $\mathbf{A}$ , as described in Section 3.1.4.
5. Obtain the **LU** factorization of  $\mathbf{A}$  and save it for repeated use.
6. Given impedance data  $\phi$  on the boundary of computational domain  $\partial\Omega$ , obtain the impedance data  $\phi^{p,q}$  on the boundary of subdomains  $\partial\Omega^{p,q}$ , for all  $p, q = 1, \dots, K$  by solving the linear system

$$\mathbf{A} \mathbf{X} = \mathbf{b}$$

where  $\mathbf{A}$  is  $N_c \times N_c$  pre-computed matrix and right hand side  $\mathbf{b} = (\phi, \mathbf{0})$ .

7. Finally obtain the solution in each subdomain  $\Omega^{p,q}$  by solving the linear system

$$\mathbf{A}_{p,q} \mathbf{X}_{p,q} = \mathbf{b}_{p,q},$$

where the right hand side  $\mathbf{b}_{p,q} = (\phi_{p,q}, 0)$ .

## 3.2 Spectral Approximation of the Boundary Integral Operator

The proposed algorithm utilizes a novel fast, high-order Nyström scheme for the solution of the boundary integral equation (15), and, thus, it suffices to describe an integration scheme that can approximate accurately the integral operator in that equation. Since, as indicated in the previous sections, the approximation grid in the interior of the volumetric region our is a union of piecewise Chebyshev grids, it is desirable for the underlying grid in the approximation of (15) to be a subset of the volumetric interior grid: otherwise an additional fast and accurate interpolation

procedure would be required for the evaluation of the integral density to the underlying quadrature points. To eliminate such additional difficulties while preserving maximal accuracy, we have used a two-dimensional analog of the rectangular polar integration scheme recently introduced in [10] for the solution of surface scattering problems in the three dimensions. The resulting procedure is described in what follows.

In a first stage, the the entire integration domain  $\partial\Omega$  is covered by a set of non-overlapping boundary patches  $\{\gamma_p\}_{p=1}^P$ , each one of which is the image of the interval  $[-1, 1]$  via a smooth invertible mapping  $\boldsymbol{\xi}_p$ . Using this covering, the integral operator in (15) can be decomposed as

$$\int_{\gamma_p} \left( \frac{\partial G_\kappa(\mathbf{x} - \mathbf{y})}{\partial \boldsymbol{\nu}(\mathbf{y})} \eta(\mathbf{y}) - G_\kappa(\mathbf{x} - \mathbf{y}) \zeta(\mathbf{y}) \right) ds(\mathbf{y}) = \sum_{p=1}^P I_p(\mathbf{x}),$$

where

$$I_p(\mathbf{x}) = \int_{\gamma_p} \left( \frac{\partial G_\kappa(\mathbf{x} - \mathbf{y})}{\partial \boldsymbol{\nu}(\mathbf{y})} \eta(\mathbf{y}) - G_\kappa(\mathbf{x} - \mathbf{y}) \zeta(\mathbf{y}) \right) ds(\mathbf{y}). \quad (39)$$

Using the parameterization  $\boldsymbol{\xi}_p$  the integral (39) can be expressed in the form

$$I_p(\mathbf{x}) = \int_{-1}^1 \left( \frac{\partial G_\kappa(\mathbf{x} - \boldsymbol{\xi}_p(t))}{\partial \boldsymbol{\nu}(\boldsymbol{\xi}_p(t))} \eta(\boldsymbol{\xi}_p(t)) - G_\kappa(\mathbf{x} - \boldsymbol{\xi}_p(t)) \zeta(\boldsymbol{\xi}_p(t)) \right) \left| \frac{\partial \boldsymbol{\xi}_p}{\partial t} \right| dt, \quad (40)$$

An adequate choice of a methodology for the accurate evaluation of (40) depends on the relative position of the target point  $\mathbf{x}$  with respect to the integration patch  $\gamma_p$ . If target point  $\mathbf{x}$  is sufficiently away from  $\gamma_p$  then the integrand in (40) is smooth and can be integrated with high-order accuracy by means of any high-order quadrature rule. On the other hand, if the target point is either close to or within the integration patch, the whole integrand either singular or near singular, and hence a specialized quadrature rule must be used for its accurate evaluation. Thus, depending upon the distance from the target point to the integration patch, the integration method consists of three different methods:

*Evaluation of non-singular integrals:* For target points  $\mathbf{x}$  sufficiently far from the integration patch we use the Clenshaw-Curtis quadrature which, as is known, enjoys high-order convergence for smooth integrands [31], and whose discretization may be taken to coincide with the restriction of the volumetric discretization to  $\partial\Omega$ .

*Evaluation of singular integrals:* For target point  $\mathbf{x}$  in the integration patch, the accurate approximation of (40) becomes challenging in view of the integrand singularity. To deal with this difficulty, we first replace the density function  $\eta$  and  $\zeta$  in (40) by its Chebyshev expansion and we thus obtain

$$I_p(\mathbf{x}) = \sum_{\ell=1}^N c_\ell I_{p,\ell}^1(\mathbf{x}) + \sum_{\ell=1}^N d_\ell I_{p,\ell}^2(\mathbf{x}), \quad (41)$$

where

$$I_{p,\ell}^1(\mathbf{x}) = \int_{-1}^1 \frac{\partial G_\kappa(\mathbf{x} - \boldsymbol{\xi}_p(t))}{\partial \boldsymbol{\nu}(\boldsymbol{\xi}_p(t))} T_\ell(t) \left| \frac{\partial \boldsymbol{\xi}_p}{\partial t} \right| dt, \quad (42)$$

$$I_{p,\ell}^2(\mathbf{x}) = \int_{-1}^1 G_\kappa(\mathbf{x} - \boldsymbol{\xi}_p(t)) T_\ell(t) \left| \frac{\partial \boldsymbol{\xi}_p}{\partial t} \right| dt, \quad (43)$$

and where  $T_\ell$  is the Chebyshev polynomial of degree  $\ell$ . The Chebyshev coefficients  $c_\ell, d_\ell$  can be obtained accurately in a fast way by means of FFT. Note that the integral in equations (42) and (43) does not depend on the density, and therefore, may be computed only once and stored for repeated use. In addition to this, evaluation of these integrals does not require interpolation, even if refined meshes are used for their evaluation, as they are analytically known in the complete domain of integration. However, evaluation of these integrals present certain difficulties owing to the weakly singular character of the integral kernel. To resolve the integrand singularity in equations (42) and (43) we utilize changes of variable whose Jacobian vanishes along with several of its derivative at the singularity point. The idea is not limited to the specific kernel presently under consideration, and it can be readily incorporated for a general class of weakly singular kernels. Thus, we present our discussion in that general context.

Letting

$$I_\ell(\mathbf{x}) = \int_{-1}^1 H_\kappa(\boldsymbol{\xi}_p(t_0) - \boldsymbol{\xi}_p(t)) T_\ell(t) \left| \frac{\partial \boldsymbol{\xi}_p}{\partial t} \right| dt, \quad (44)$$

where  $\mathbf{x} = \boldsymbol{\xi}_p(t_0)$  and  $H_\kappa(\boldsymbol{\xi}_p(t_0) - \boldsymbol{\xi}_p(t))$  is any weakly singular kernel, we re-express  $I_\ell$  in the form

$$I_\ell(\mathbf{x}) = \int_{-1}^{t_0} H_\kappa(\boldsymbol{\xi}_p(t_0) - \boldsymbol{\xi}_p(t)) T_\ell(t) \left| \frac{\partial \boldsymbol{\xi}_p}{\partial t} \right| dt + \int_{t_0}^1 H_\kappa(\boldsymbol{\xi}_p(t_0) - \boldsymbol{\xi}_p(t)) T_\ell(t) \left| \frac{\partial \boldsymbol{\xi}_p}{\partial t} \right| dt. \quad (45)$$

Both the first and second integrands in (45) are singular at  $t = t_0$ . To resolve the singularity we use the change of variables [14]

$$\tau = t_0 - \frac{1+t_0}{\pi} \omega_k \left[ \frac{\pi}{2}(-t+1) \right]$$

and

$$\tau = t_0 + \frac{1-t_0}{\pi} \omega_k \left[ \frac{\pi}{2}(t+1) \right]$$

in first and second integrals in (45), respectively. Here,

$$\omega_k(s) = 2\pi \frac{[v(s)]^k}{[v(s)]^k + [v(2\pi - s)]^k}, \quad 0 \leq s \leq 2\pi,$$

where

$$v(s) = \left( \frac{1}{k} - \frac{1}{2} \right) \left( \frac{\pi - s}{\pi} \right)^3 + \frac{1}{k} \left( \frac{s - \pi}{\pi} \right) + \frac{1}{2},$$

and  $k > 1$  is an integer. It is easy to check that the Jacobians of these change of variables vanishes up to order  $k - 1$  at the singular point  $t = t_0$ , which renders smooth integrand which can be integrated to high-order by means of the Clenshaw-Curtis quadrature.

*Evaluation of near-singular integrals:* This case arises when the target point  $\mathbf{x}$  is “very close” to, but outside the integration patch  $\gamma_p$ . In this case, while the integrand in (40) is, strictly speaking, non-singular, its numerical integration poses similar challenges to the singular case. To alleviate this issue, we project the target point into the closest point to it on the integration patch and then follow the same strategy used for singular integration by treating the projection point as the singular point.

### 3.3 Overall hybrid solver

The main lines of the proposed method are presented in what follows:

1. Replace the discontinuous refractivity  $n^2(\mathbf{x})$  in equation (13) by its Fourier smoothing  $1 - m^F(\mathbf{x})$  as discussed in subsubsection 3.1.1.
2. Construct an initial guess for the impedance data  $\phi$  in equation (14) and solve the BVP (13)–(14) by means of the direct solution technique discussed in Section 3.1.2.
3. Using either the solution obtained in step 2 or any improved guess for  $\phi$  produced by the linear-algebra solver GMRES, compute the action of impedance operator  $T_{\text{int}}$  on  $\phi$  to obtain  $(I + T_{\text{int}})[\phi]$  and  $(I - T_{\text{int}})[\phi]$  on  $\partial\Omega$ .
4. Evaluate  $\mathcal{A}_{\text{ext}}^{\text{int}}[\phi]$  as well as the left hand side of equation (15), on the discretization of  $\partial\Omega$ , for the density values  $(I + T_{\text{int}})[\phi]$  and  $(I - T_{\text{int}})[\phi]$ .
5. Provide the resulting residual (equal to the difference between the left-hand and the right-hand sides in (15) to the GMRES algorithm, to obtain a new approximation for the density  $\phi$ .
6. Check for convergence to a given prescribed tolerance, and iterate by returning to step 3 until convergence is achieved.

## 4 Numerical results

This section presents numerical tests and examples that demonstrate the performance of the scattering solvers introduced in the Section 3, with an emphasis on problems containing discontinuous refractivities. All numerical results presented in this section were produced by means of a C++ implementation of the algorithms described in Section 3, together with the Multifrontal solver for the solution of linear system at different steps of the algorithm, on a single core of an Intel i7-4600M processor. The relative error (in the near field) reported here are computed according to

$$\varepsilon_{\infty} = \frac{\max_{1 \leq i \leq N} |u^{\text{exact}}(\mathbf{x}_i) - u^{\text{approx}}(\mathbf{x}_i)|}{\max_{1 \leq i \leq N} |u^{\text{exact}}(\mathbf{x}_i)|}.$$

In all of the tabulated results, the acronym “numIt” denotes the number of GMRES iterations required to achieve the desired accuracy and “Order” denotes the numerical order of convergence.

**Example 4.1.** (*Spectral Convergence for Boundary Integral Operator*)

This example illustrates the spectral convergence of the proposed rectangular integration technique (proposed in Section 3.2). For our example we evaluate numerically the integral

$$2 \int_{\partial\Omega} \left\{ G_{\kappa}(\mathbf{x} - \mathbf{y}) \frac{\partial u(\mathbf{y})}{\partial n(\mathbf{y})} - \frac{G_{\kappa}(\mathbf{x} - \mathbf{y})}{\partial n(\mathbf{y})} u(\mathbf{y}) \right\} d\mathbf{y}, \quad (46)$$

for  $x \in \partial\Omega$  and with density  $u = u^i$  (where  $u^i$  is the solution of free space Helmholtz equation (2))—for which the exact value of the integral is known. To demonstrate the spectral convergence we have

computed the integral (46) over the boundary of square region  $\Omega = \{(x, y) | -1.5 \leq x, y \leq 1.5\}$  with  $u^i(\mathbf{x}) = e^{i\kappa x}$  and  $\kappa = 5\pi$ , over successive discretizations; the corresponding results are tabulated in Table 1.

N	#of Patches	$\kappa$	$\epsilon_\infty$	Order
6	8	$5\pi$	2.72e-00	-
12	8	$5\pi$	5.11e-01	2.41e+00
24	8	$5\pi$	2.74e-03	7.54e+00
48	8	$5\pi$	3.89e-08	16.10e+00
96	8	$5\pi$	4.94e-11	9.62e+00
192	8	$5\pi$	1.16e-13	8.73e+00

Table 1: Convergence study. Errors are reported for the rectangular integration method introduced in Section 3.2. Numerical errors were obtained by comparison against closed-form exact values.

The proposed integration scheme additionally remains accurate for arbitrarily large frequencies. To illustrate this, we have computed integral (46) for various wavenumbers; the corresponding results are tabulated in Table 2 for experiments with a fixed number of points per wavelength. Table 2 shows that, as claimed, the proposed scheme does not deteriorate as the wavenumber is increased while keeping a constant number of points per wavelength.

N	# of Patches	$\kappa$	PPW	Rel. Error
30	12	$10\pi$	6	2.34e-05
30	24	$20\pi$	6	2.60e-05
30	48	$40\pi$	6	2.65e-05
30	96	$80\pi$	6	2.91e-05
30	192	$160\pi$	6	3.00e-05
30	384	$320\pi$	6	3.11e-05

Table 2: Illustration of the proposed spectrally accurate integration scheme for large wavenumbers with a fixed number of points per wavelength.

**Example 4.2.** (*Scattering by Circular Inclusion* )

In this example, we corroborate the expected quadratic convergence of the overall algorithm for penetrable inhomogeneous media with discontinuous refractivity via an application to the canonical problem of scattering by a circular (cylindrical) domain. For this experiment the diameter of the circular inhomogeneity equals two and we have selected  $n^2(\mathbf{x}) = 2$  for  $\mathbf{x} \in \mathcal{D}$  and one otherwise, and an incident wave of the form  $u^i(\mathbf{x}) = J_0(\kappa|\mathbf{x}|)$ , where  $\kappa = 5$  and where  $J_0$  is the Bessel function of the first kind of order zero. With this incident wave the solution of the problem (2)-(3) can be computed analytically [4]. For the sake of comparison we have computed the numerical solution with and without Fourier smoothing for different levels of discretization; the corresponding numerical results are presented in Table (3). As indicated above, these results clearly corroborate the quadratic convergence of the algorithm for discontinuous refractivity profiles. We also see that, by Fourier smoothing of discontinuous refractivity we have achieved significant accuracy in the solution.

$n_1 \times n_2$	# of Patches	$\kappa$	Rel. Error(Without FS)	Rel. Error(With FS)	Order
$11 \times 11$	$2 \times 2$	$5\pi$	8.31e-01	8.44e-01	-
$11 \times 11$	$4 \times 4$	$5\pi$	1.12e-01	9.66e-02	3.12
$11 \times 11$	$8 \times 8$	$5\pi$	4.60e-02	1.30e-02	2.89
$11 \times 11$	$16 \times 16$	$5\pi$	5.65e-03	2.04e-03	2.67
$11 \times 11$	$32 \times 32$	$5\pi$	4.46e-03	3.28e-04	2.64
$11 \times 11$	$64 \times 64$	$5\pi$	1.37e-03	4.46e-05	2.87
$11 \times 11$	$128 \times 128$	$5\pi$	4.02e-04	9.74e-06	2.19

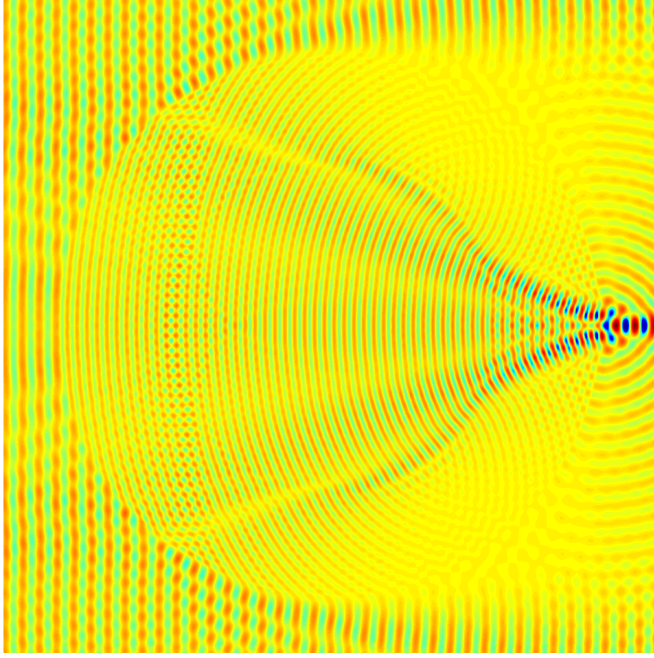
Table 3: Convergence Study: Illustration of the quadratic convergence of the proposed algorithm from a problem of scattering by a circular inclusion of diameter two with  $u^i(\mathbf{x}) = J_0(\kappa|\mathbf{x}|)$  and  $n^2(\mathbf{x}) = 2$  if  $\mathbf{x} \in \mathcal{D}$  and one otherwise.

Our algorithm can also deal with large scale frequency problems. To demonstrate this we present Table 4 which contains numerical results corresponding to certain large-scale discontinuous refractivity problems. This table shows that the proposed method achieves accuracies of the order of three digits for a discontinuous-refractivity the scatterer whose diameter is  $97 \cdot \lambda_{\text{int}}$ , where  $\lambda_{\text{int}}$  denotes the wavelength in the high refractivity region. (Note that  $\lambda_{\text{int}} = \frac{2\pi}{n\kappa}d$ , where  $d$  is the diameter of the inhomogeneity.)

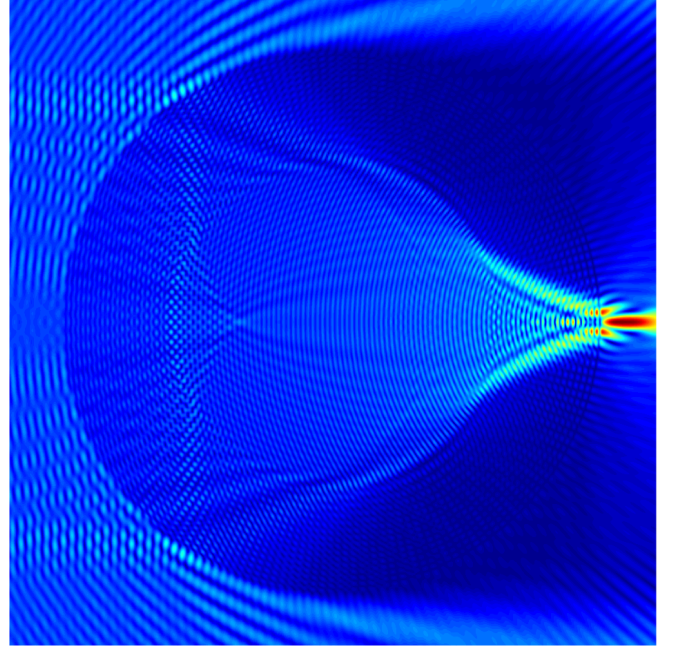
$\kappa$	# of $\lambda_{\text{int}}$	PPW	Rel. Error	# Iter.	Time(Sec.)	
					pre-comp	per. It.
100	32	12	2.49e-03	41	130	.5
200	64	13	1.51e-03	45	1427	1.99
300	97	11	5.74e-03	135	2286	2.83

Table 4: High-frequency scattering problem. Numerical solution for a problem of scattering by a circular inclusion of diameter one with  $u^i(\mathbf{x}) = J_0(\kappa|\mathbf{x}|)$  and  $n^2(\mathbf{x}) = 4$  for  $\mathbf{x} \in \mathcal{D}$  and one otherwise. The numerical errors are evaluated by comparison against the exact analytical solution.

Figure 2 displays simulation results for  $u^i(\mathbf{x}) = \exp(i\kappa x)$ ,  $\kappa = 100$  and  $n^2(\mathbf{x}) = 3$  for  $\mathbf{x} \in \mathcal{D}$  and one otherwise, where  $\mathcal{D}$  is a circular inclusion of unit diameter. In terms of interior wavelength, the diameter of inhomogeneity is  $55\lambda_{\text{int}}$ . Using 12 points per wave length the method achieves three digits of accuracy in the near field in a nine-minute single-core computation.



(a) Real part of the total Field  $u$ .



(b) Absolute value of the total field  $u$ .

Figure 2: Scattering of a plane wave  $\exp(i\kappa x)$  by a penetrable circular inclusion with diameter equal to  $56\lambda_{\text{int}}$  and  $n^2(\mathbf{x}) = 3$  if  $\mathbf{x} \in \mathcal{D}$  and one otherwise, where  $\mathcal{D}$  is the circular inclusion of unit diameter. Using 12 points per wavelength the algorithm produced three-digit accuracy in a nine minutes single-core computation.

**Example 4.3.** (*Scattering by Gaussian Refractivity* )

The proposed algorithm is not restricted to constant material properties, of course, and our next example demonstrates the properties of the solver when applied to a scatterer containing continuously variable material properties as well as discontinuities across the material interface. The interior refractive-index function selected is the Gaussian function

$$n^2(\mathbf{x}) = \begin{cases} 3 + 2e^{-4|\mathbf{x}|^2} & \text{if } \mathbf{x} \in \mathcal{D}, \\ 1 & \text{otherwise,} \end{cases} \quad (47)$$

where  $\mathcal{D}$  is circular inclusion of unit radius. To study the convergence behavior, once again, we compute the total field  $u$  under the plane wave incidence  $u^i(\mathbf{x}) = \exp(i\kappa x)$ . Since analytical solutions are not available in this case, we use numerical solution obtained on a finer grids for reference.

The numerical results reported in Table 5 once again illustrate, in particular, the quadratic convergence of the algorithm.

$n_1 \times n_2$	# of Patches	$\kappa$	Rel. Error(Without FS)	Rel. Error(With FS)	Order
$11 \times 11$	$2 \times 2$	$2\pi$	4.66e-02	4.60e-02	-
$11 \times 11$	$4 \times 4$	$2\pi$	1.55e-02	8.19e-03	2.49
$11 \times 11$	$8 \times 8$	$2\pi$	6.64e-03	3.43e-03	1.25
$11 \times 11$	$16 \times 16$	$2\pi$	4.19e-03	2.43e-04	3.81
$11 \times 11$	$32 \times 32$	$2\pi$	5.21e-04	8.09e-05	1.57
$11 \times 11$	$64 \times 64$	$2\pi$	3.74e-04	1.60e-05	2.33

Table 5: Convergence Study: Illustration of quadratic convergence of the proposed algorithm for scattering by a Gaussian refractivity scatterer given in (47). An incident plane wave incoming from the positive  $x$ -axis was used.

Figure 3 displays results of the Gaussian refractivity experiment. For the case depicted in the figure the diameter of inhomogeneity is  $36\lambda_{\text{int}}$ , for which the algorithm achieved three-digit accuracy in the near field by using 12 points per wavelengths in a four minute single-core computation.

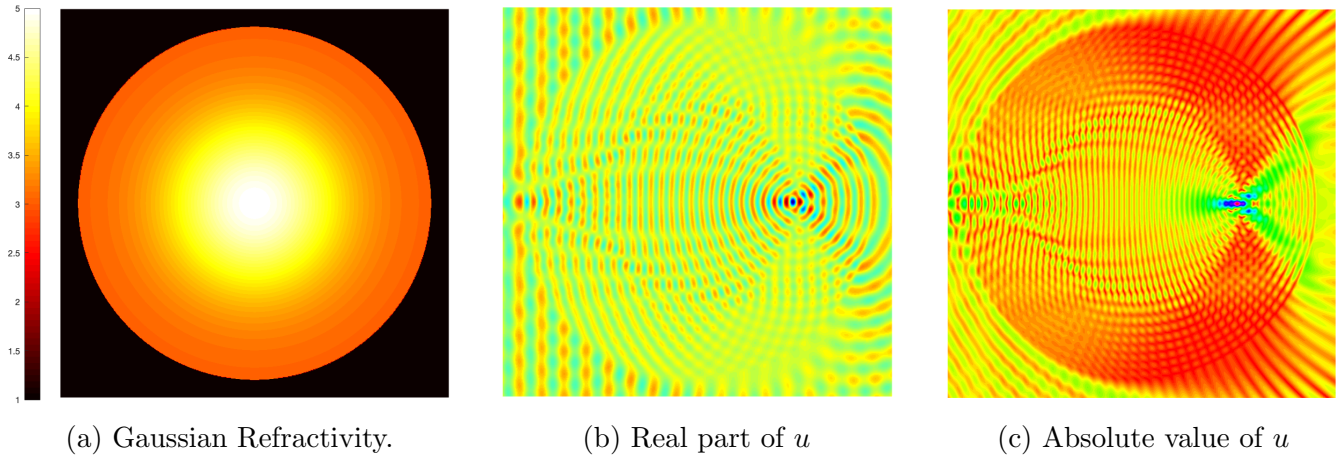


Figure 3: Scattering of a plane wave  $\exp(i\kappa x)$  by a the Gaussian refractivity profile (47) with  $\kappa = 50$ . Using 12 points per wavelength the algorithm produced three-digit accuracy in a four-minute computation.

**Example 4.4.** (*Scattering by geometries containing corners and cusps*)

None of the algorithmic components, nor the resulting accuracies in the proposed method, are constrained in any way by the geometry of the scatterer. Without any additional effort, the approach can easily deal with arbitrarily complicated geometries. To demonstrate this, we consider two additional geometries, containing corner- and cusp-singularities, respectively. Once again the accuracy of any one solution is evaluated by comparison with results obtained on finer grids. In both cases we compute the near field solution  $u$  under the plane wave incidence  $u^i(\mathbf{x}) = \exp(i\kappa x)$ .

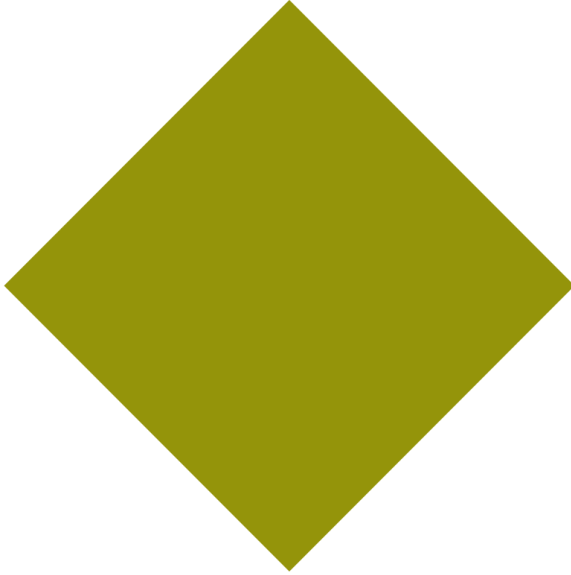
$n_1 \times n_2$	# of Patches	$\kappa$	Rel. Error	Order
$12 \times 12$	$4 \times 4$	$6\pi$	6.66e-02	-
$12 \times 12$	$8 \times 8$	$6\pi$	7.72e-03	3.10e+00
$12 \times 12$	$16 \times 16$	$6\pi$	1.17e-03	2.72e+00
$12 \times 12$	$32 \times 32$	$6\pi$	1.12e-04	3.38e+00
$12 \times 12$	$64 \times 64$	$6\pi$	1.13e-05	3.30e+00

Table 6: Convergence Study: Illustration of quadratic convergence of the proposed algorithm for a geometry containing a corner singularity.

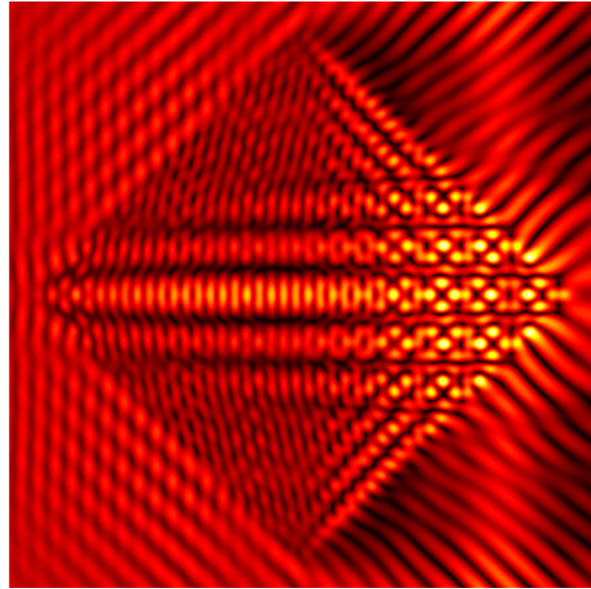
Table 6 presents numerical results for the problem of scattering by the scatterer geometry depicted in Figure 4(a), with  $n^2(\mathbf{x}) = 2$  if  $\mathbf{x}$  lies in the inhomogeneity region  $\mathcal{D}$  and one otherwise. The computed near field for  $\kappa = 50$ , which was determined to be accurate up to four digits, is displayed in Figure 4(b). Table 7, in turn, presents numerical results for the scatterer depicted in Figure 5(a), which equals the region contained between four unit discs centered at  $(1,1)$ ,  $(1,-1)$ ,  $(-1,1)$  and  $(-1,-1)$  respectively. For this experiment we have taken  $n^2(\mathbf{x}) = 2$  if  $\mathbf{x} \in \mathcal{D}$  and one otherwise. Figure 5(b) displays the near field for the same geometry with  $\kappa = 20\pi$  and  $n^2(\mathbf{x}) = 16$  if  $\mathbf{x} \in \mathcal{D}$  and one otherwise—thus yielding a scatterer  $80\lambda_{\text{int}}$  in size. A two-digit accurate solution was obtained using merely nine points per wavelength in this case.

$n_1 \times n_2$	# of Patches	$\kappa$	Rel. Error(With FS)	Order
$12 \times 12$	$2 \times 2$	$4\pi$	4.95e-01	-
$12 \times 12$	$4 \times 4$	$4\pi$	4.80e-02	3.36
$12 \times 12$	$8 \times 8$	$4\pi$	9.46e-03	2.34
$12 \times 12$	$16 \times 16$	$4\pi$	1.79e-03	2.40
$12 \times 12$	$32 \times 32$	$4\pi$	3.56e-04	2.32
$12 \times 12$	$64 \times 64$	$4\pi$	6.33e-05	2.49

Table 7: Convergence Study: Illustration of quadratic convergence of the proposed algorithm for a geometry containing a cusp singularity.

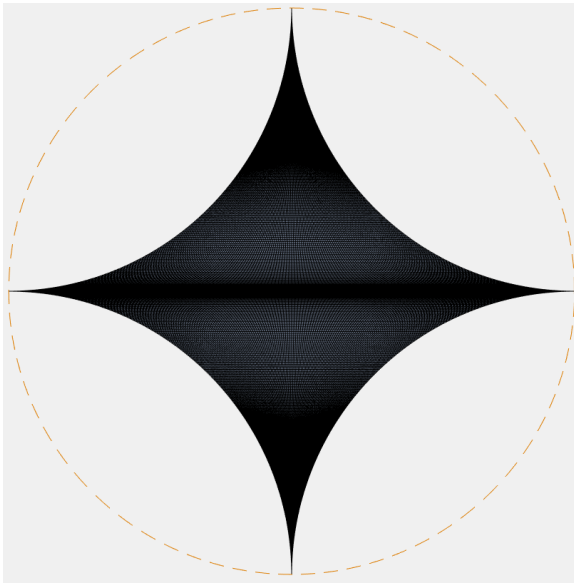


(a) Square shape geometry

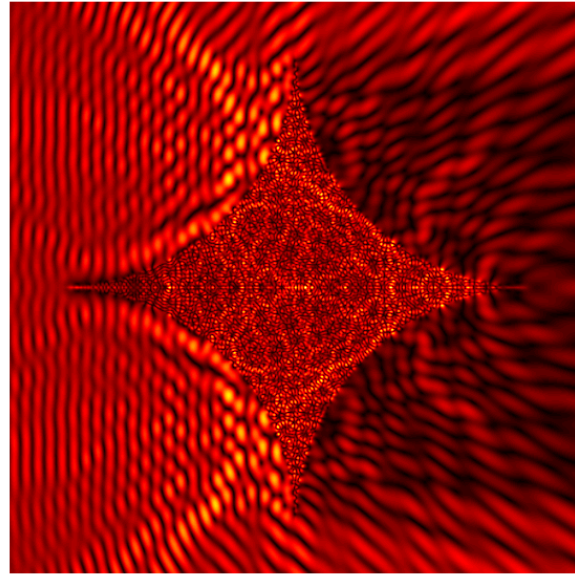


(b) Absolute value of the total field  $u$ .

Figure 4: Scattering by a geometry containing corner singularities, with  $n^2(\mathbf{x}) = 2$  for  $\mathbf{x} \in \mathcal{D}$  and one otherwise. For this experiment the incident field  $u^i(\mathbf{x}) = \exp(i\kappa x)$  with  $\kappa = 50$  was used. Four digits of accuracy were obtained in the near field solution.



(a) Star-shaped geometry with cusp



(b) Absolute value of total field  $u$

Figure 5: Scattering by a geometry containing cusp singularities, with  $n^2(\mathbf{x}) = 16$  if  $\mathbf{x} \in \mathcal{D}$  and one otherwise. For this experiment the incident field  $u^i(\mathbf{x}) = \exp(i\kappa x)$  with  $\kappa = 20\pi$  was used. Two digits of accuracy were obtained in the near field solution on the basis of nine points per interior wavelength.

## 5 Conclusions

This paper introduced a new methodology for solutions of two-dimensional problems of scattering by penetrable inhomogeneous media with possibly discontinuous refractivity. The solver achieves high-order convergence for smooth refractivities and, to the best of our knowledge, it is the first direct solver which gives second order convergence for discontinuous refractivity which has been demonstrated for problems of high-frequency. Without extra additions the method can easily handle scatterers with geometric singularities such as corners and cusps. So far, we have considered only inhomogeneous scattering by acoustic waves. Extensions to electromagnetic and elastic wave scattering problems, as well as three-dimensional configurations are envisioned.

## Acknowledgements

This work was supported by NSF and AFOSR through contracts DMS-1411876 and FA9550-15-1-0043, and by the NSSEFF Vannevar Bush Fellowship under contract number N00014-16-1-2808.

## References

- [1] JC Aguilar and Yu Chen. A high-order, fast algorithm for scattering calculation in two dimensions. *Computers & Mathematics with Applications*, 47(1):1–11, 2004.
- [2] Sivaram Ambikasaran, Carlos Borges, Lise-Marie Imbert-Gerard, and Leslie Greengard. Fast, adaptive, high-order accurate discretization of the Lippmann–Schwinger equation in two dimensions. *SIAM Journal on Scientific Computing*, 38(3):A1770–A1787, 2016.
- [3] Akash Anand, Ambuj Pandey, BV Rathish Kumar, and Jagabandhu Paul. An efficient high-order nyström scheme for acoustic scattering by inhomogeneous penetrable media with discontinuous material interface. *Journal of Computational Physics*, 311:258–274, 2016.
- [4] Fredrik Andersson and Anders Holst. A fast, bandlimited solver for scattering problems in inhomogeneous media. *Journal of Fourier Analysis and Applications*, 11(4):471–487, 2005.
- [5] Richard C Aster, Brian Borchers, and Clifford H Thurber. *Parameter estimation and inverse problems*. Elsevier, 2018.
- [6] Ivo M Babuska and Stefan A Sauter. Is the pollution effect of the fem avoidable for the Helmholtz equation considering high wave numbers? *SIAM Journal on numerical analysis*, 34(6):2392–2423, 1997.
- [7] Alvin Bayliss, Charles I Goldstein, and Eli Turkel. The numerical solution of the Helmholtz equation for wave propagation problems in underwater acoustics. *Computers & Mathematics with Applications*, 11(7-8):655–665, 1985.
- [8] Alvin Bayliss, Charles I Goldstein, and Eli Turkel. On accuracy conditions for the numerical computation of waves. *Journal of Computational Physics*, 59(3):396–404, 1985.

- [9] Alfredo Bermúdez, Luis Hervella-Nieto, Andrés Prieto, R Rodri, et al. An optimal perfectly matched layer with unbounded absorbing function for time-harmonic acoustic scattering problems. *Journal of Computational Physics*, 223(2):469–488, 2007.
- [10] Oscar P Bruno and Emmanuel Garza. A Chebyshev-based rectangular-polar integral solver for scattering by general geometries described by non-overlapping patches. *arXiv preprint arXiv:1807.01813*, 2018.
- [11] Oscar P Bruno and E McKay Hyde. An efficient, preconditioned, high-order solver for scattering by two-dimensional inhomogeneous media. *Journal of Computational Physics*, 200(2):670–694, 2004.
- [12] Oscar P Bruno and E McKay Hyde. Higher-order Fourier approximation in scattering by two-dimensional, inhomogeneous media. *SIAM Journal on Numerical Analysis*, 42(6):2298–2319, 2005.
- [13] Oscar P Bruno and Leonid A Kunyansky. A fast, high-order algorithm for the solution of surface scattering problems: basic implementation, tests, and applications. *Journal of Computational Physics*, 169(1):80–110, 2001.
- [14] David Colton and Rainer Kress. *Inverse acoustic and electromagnetic scattering theory*, volume 93. Springer, 2012.
- [15] Timothy A Davis. Algorithm 832: Umfpack v4. 3—an unsymmetric-pattern multifrontal method. *ACM Transactions on Mathematical Software (TOMS)*, 30(2):196–199, 2004.
- [16] Ran Duan and Vladimir Rokhlin. High-order quadratures for the solution of scattering problems in two dimensions. *Journal of Computational Physics*, 228(6):2152–2174, 2009.
- [17] Björn Engquist and Andrew Majda. Absorbing boundary conditions for numerical simulation of waves. *Proceedings of the National Academy of Sciences*, 74(5):1765–1766, 1977.
- [18] Björn Engquist and Lexing Ying. Sweeping preconditioner for the Helmholtz equation: hierarchical matrix representation. *Communications on pure and applied mathematics*, 64(5):697–735, 2011.
- [19] Oliver G Ernst and Martin J Gander. Why it is difficult to solve Helmholtz problems with classical iterative methods. In *Numerical analysis of multiscale problems*, pages 325–363. Springer, 2012.
- [20] Adrianna Gillman, Alex H Barnett, and Per-Gunnar Martinsson. A spectrally accurate direct solution technique for frequency-domain scattering problems with variable media. *BIT Numerical Mathematics*, 55(1):141–170, 2014.
- [21] Marcus J Grote and Joseph B Keller. On nonreflecting boundary conditions. *Journal of Computational Physics*, 122(2):231–243, 1995.
- [22] Thomas Hagstrom and Timothy Warburton. A new auxiliary variable formulation of high-order local radiation boundary conditions: corner compatibility conditions and extensions to first-order systems. *Wave motion*, 39(4):327–338, 2004.

- [23] E McKay Hyde and Oscar P Bruno. A fast, higher-order solver for scattering by penetrable bodies in three dimensions. *Journal of Computational Physics*, 202(1):236–261, 2005.
- [24] A Kirsch and P Monk. Convergence analysis of a coupled finite element and spectral method in acoustic scattering. *IMA journal of numerical analysis*, 10(3):425–447, 1990.
- [25] Andreas Kirsch and Peter Monk. An analysis of the coupling of finite-element and nyström methods in acoustic scattering. *IMA Journal of numerical analysis*, 14(4):523–544, 1994.
- [26] Peter Kuchment. *The Radon transform and medical imaging*, volume 85. SIAM, 2014.
- [27] F Lanzara, V Maz’ya, and G Schmidt. Numerical solution of the Lippmann–Schwinger equation by approximate approximations. *Journal of Fourier Analysis and Applications*, 10(6):645–660, 2004.
- [28] Fei Liu and Lexing Ying. Sparsify and sweep: An efficient preconditioner for the Lippmann–Schwinger equation. *SIAM Journal on Scientific Computing*, 40(2):B379–B404, 2018.
- [29] Ambuj Pandey and Akash Anand. Improved convergence of fast integral equation solvers for acoustic scattering by inhomogeneous penetrable media with discontinuous material interface. *Journal of Computational Physics*, 376:767–785, 2019.
- [30] Gennadi Vainikko. Fast solvers of the Lippmann-Schwinger equation. In *Direct and inverse problems of mathematical physics*, pages 423–440. Springer, 2000.
- [31] Jörg Waldvogel. Fast construction of the fejer and Clenshaw–Curtis quadrature rules. *BIT Numerical Mathematics*, 46(1):195–202, 2006.
- [32] Shen Wang, Maarten V de Hoop, and Jianlin Xia. On 3d modeling of seismic wave propagation via a structured parallel multifrontal direct helmholtz solver. *Geophysical Prospecting*, 59(5):857–873, 2011.
- [33] Lexing Ying. Sparsifying preconditioner for the Lippmann–Schwinger equation. *Multiscale Modeling & Simulation*, 13(2):644–660, 2015.
- [34] Leonardo Zepeda-Núñez and Hongkai Zhao. Fast alternating bidirectional preconditioner for the 2d high-frequency Lippmann–Schwinger equation. *SIAM Journal on Scientific Computing*, 38(5):B866–B888, 2016.